CrossMark

# High Rate Lithium Ion Battery with Niobium Tungsten Oxide Anode

Yumi Kim,[1] Quentin Jacquet,[1] Kent J. Griffith,[2,*] Jeongjae Lee,[1] Sunita Dey,[1] Bernardine L. D. Rinkel,[1] and Clare P. Grey[1,**,z]

[1]*Department of Chemistry, University of Cambridge, Cambridge, CB2 1EW, United Kingdom*
[2]*Departments of Chemistry and Materials Science and Engineering, Northwestern University, Evanston, Illinois 60208, United States of America*

Highly stable lithium-ion battery cycling of niobium tungsten oxide ($Nb_{16}W_5O_{55}$, NWO) is demonstrated in full cells with cathode materials $LiNi_{0.6}Mn_{0.2}Co_{0.2}O_2$ (NMC-622) and $LiFePO_4$ (LFP). The cells show high rate performance and long-term stability under 5 C and 10 C cycling rates with a conventional carbonate electrolyte without any additives. The degradation of the cell performance is mainly attributed to the increased charge transfer resistance at the NMC side, consistent with the ex situ XRD and XPS analysis demonstrating the structural stability of NWO during cycling together with minimal electrolyte decomposition. Finally, we demonstrate the temperature-dependent performance of this full cell at 10, 25 and 60 °C and confirm, using *operando* XRD, that the structural change of the NWO material during lithiation/de-lithiation at 60 °C is very similar to its behaviour at 25 °C, reversible and with a low volume change. With the merits of high rate performance and long cycle life, the combination of NWO and a commercial cathode represents a promising, safe battery for fast charge/discharge applications.

Supplementary material for this article is available online

The growing global energy demand, together with the quest for clean and renewable sources of energy, drives research into Li-ion batteries with high energy density and high rate performance.[1–3] In many portable electronics and electric vehicles, fast charging and high power density are two of the key requirements.[4–6] In this regard, $LiFePO_4$ (LFP) has been extensively used as a stable cathode material allowing for high currents in a full cell; it however exhibits a lower working voltage (vs Li) and practical capacity than Ni-rich cathodes such as $LiNi_{0.6}Mn_{0.2}Co_{0.2}O_2$ (NMC-622).[7–10] On the anode side, graphite is used commercially due to its low cost, wide availability and low delithiation voltage (vs Li); however, it has electrolyte stability issues at low voltages resulting in the formation of a passivating layer.[11,12] This surface–electrolyte interphase (SEI) layer is known to be an essential component for graphite anodes; however, it consumes $Li^+$ during formation, lowering the initial coulombic efficiency of the cell. Moreover, graphite has the serious issue of Li plating at high rates and/or low temperatures leading to the formation of dendrites negatively impacting the cycle life, rate capability and safety of the cell. $Li_4Ti_5O_{12}$ (LTO), having a higher working voltage (1.55 V vs Li) hence reduced SEI formation and dendrite growth, is commonly suggested as a promising candidate for high power applications. However, it needs to be nanosized to access high rates, leading to a low volumetric energy density of LTO-based cells, and problematic evolution of $H_2$ and $CO_2$ gases upon cycling.[13–16] Clearly, novel anode materials with high rate performance are needed for safe Li-ion cells with high energy and power densities.

Recently, our group has reported that $Nb_{16}W_5O_{55}$ (NWO) which crystallizes in a $ReO_3$ block-type structure, featuring 2D tunnels suitable for Li conduction shows promising performance for high-rate lithium-ion energy storage even with micro-sized particles.[17] Many other studies of compounds having different stoichiometries but similar structural motifs have also shown excellent high rate performance in half-cell configurations and for electrodes having a high conductive carbon content (>10%) and low loading (<2 mg cm$^{-2}$).[18–21] Here we

present the full cell performance of more practical electrodes of NWO in combination with two commercial cathode materials for high rate Li-ion batteries: LFP and NMC.

## Experimental

***Electrode preparation.***—NWO powder was synthesized as previously reported in the literature.[17] NMC-622 (Targray) and a commercial source of carbon-coated LFP with 0.5 um particle size were used as cathodes (Fig. S1 available online at stacks.iop.org/JES/168/010525/mmedia). The XRD analysis of all active materials confirm that they are phase pure as shown in Fig. S2. High loadings electrodes were prepared mixing Super P carbon (TIMCAL) and polyvinylidene fluoride (PVdF; Kynar) dispersed in *N*-methyl-2-pyrrolidone. All slurries were composed of 90% active material, 5% super P and 5% PVdF binder, and the mixing was conducted with a Thinky Mixer 250. The NMC and LFP electrodes were dried in an oven at 80 °C for 2 h in a dry room, and the NWO electrodes were dried in an oven at 60 °C overnight under ambient atmosphere. All electrodes were calendared at room temperature and the resulting electrode porosities were in the range of 35%–45%. The electrodes loadings were 8.0–8.3 mg cm$^{-2}$ (NMC), 8.4–8.7 mg cm$^{-2}$ (LFP) and 8.8–9.4 mg cm$^{-2}$ (NWO) with 1 cm$^2$ electrode size. Low loading electrodes were prepared in a similar fashion but with a different composition namely having 10% Li250 carbon (Denka), 10% PVdF (Kynar) dispersed in *N*-methyl-2-pyrrolidone, and 80% of active material. The resulting active material loading were 4.0 mg cm$^{-2}$ for NMC, 3.8 mg cm$^{-2}$ for LFP and 4.4 mg cm$^{-2}$ for NWO.

***Electrochemical characterization.***—All electrochemical measurements were evaluated with 2032-type stainless steel coin cells. Prepared cathode and anode electrodes were dried at 100 °C for 3 h under vacuum, then transferred into an argon-filled glove box (MBraun) without exposure to air. Full cells were assembled in the glove box with LP30 electrolyte (Sigma-Aldrich, battery grade), which is composed of 1.0 M lithium hexafluorophosphate ($LiPF_6$) in ethylene carbonate (EC): dimethyl carbonate (DMC) (1:1 v/v). A polyethylene separator (Toray) was used after drying at 40 °C for 2 h under vacuum. For electrolyte analyses, glass fiber filter paper (Whatman, GE) was used as the separator. The filter was also dried

*Electrochemical Society Member.
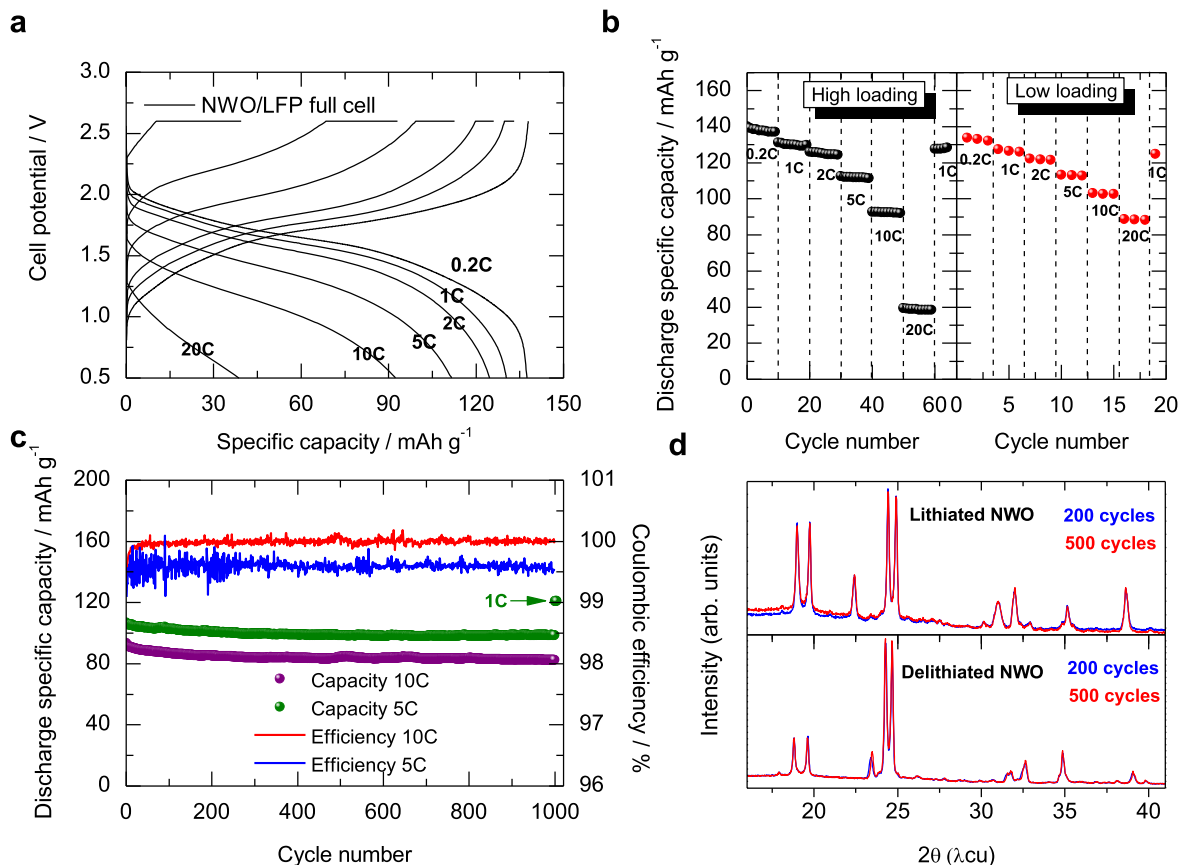**Electrochemical Society Fellow.
zE-mail: cpg27@cam.ac.uk

**Figure 1.** (a) Cell voltage profiles of the high loading NWO/LFP full cell at 0.2 C, 1 C, 2 C, 5 C, 10 C and 20 C, (b) Rate performance of the high loading and low loading NWO/LFP full cells and (c) Discharge capacity and coulombic efficiency (C.E.) plots from long-term cycling of the high loading NWO/LFP cell operated at 25 °C at 5 C and 10 C (d) XRD patterns of ex situ NWO electrodes cycled in a LFP/NWO full cell at 5 C for 200 and 500 cycles and stopped after charge (lithiated NWO) and discharge (delithiated NWO).

at 150 °C under vacuum in a drying oven (Buchi). For half cells, Li metal chip (250 $\mu$m, PI-KEM), LP30 electrolyte and glass fiber filter were used as the counter electrode, electrolyte and separator, respectively. Galvanostatic electrochemical tests were conducted at various current densities by using a galvanostat/potentiostat (BioLogic) in a temperature-controlled oven at 10, 25 and 60 °C. All cells had a negative-to-positive capacity ratio of 1.1–1.2, which is calculated based on the practical capacities of the active materials, i.e. 171.3 mAh g$^{-1}$ for NWO, 175 mAh g$^{-1}$ for NMC and 165 mAh g$^{-1}$ for LFP. Full cell capacities in this study are calculated by active material mass of the cathode. In full cell tests, charge was performed under constant current and constant voltage mode (CC/CV, with the CV step limited by specific current to > C/10) and discharge was operated under constant current (CC) mode. For symmetrical cell tests, two full cells having the same loading were operated at 0.2 C, and impedance was measured at 2.0 V during the charging step. Frequencies from 1 MHz to 100 mHz were scanned with an applied amplitude of 10 mV. Afterwards, cells were disassembled in the glove box, and two symmetric cells were assembled with fresh LP30 electrolyte. Electrochemical impedance was measured again on the symmetric cells under the same conditions. For half cells, working voltages were 1–3 V vs Li/Li$^+$(NWO), 3.0–4.2 V vs Li/Li$^+$ (NMC), and 2.8–4.0 V vs Li/Li$^+$ (LFP).

***Characterization of electrodes.***—For characterization, ex situ samples were prepared as follow: cells were disassembled and rinsed with DMC, then dried in the glovebox pre-chamber under vacuum. Electrode microstructures were analyzed by scanning electron microscopy (MIRA3, TESCAN) at 5.0 kV with secondary electron detection. Electron microscopy images of the pristine electrodes of NWO, NMC and LFP are shown Fig. S1. X-ray diffraction patterns

of pristine and cycled electrodes were obtained in Bragg–Brentano geometry (Empyrean, Panalytical) at ambient temperature with a Cu-K$\alpha$ source. The *operando* XRD measurement at high temperature was performed in the same instrument using a home-made cell with a Be window and heating bars. The scan time was 10 min. Lattice parameters, phase and purity of the material were determined by Rietveld refinement (or Lebail on the NWO material due to its large unit cell) using the FullProf software.[22] X-ray photoelectron spectroscopy (XPS) was carried out with a Thermo Fisher Scientific instrument with a monochromated Al-K$\alpha$ X-ray source (*hν* of 1468.7 eV). Samples were adhered to conductive carbon film taped onto an airtight transfer chamber equipped with an X-ray-transparent window.

***Characterization of electrolyte.***—For electrolyte analyses, the glass fiber separator was extracted from cell and soaked in 0.75 ml of DMSO-d$_6$ (Sigma-Aldrich, 99.9 atom% D, 99% CP) for 5 min, after which the solution was transferred into an air-tight J-Young tube. $^1$H, $^{19}$F{$^1$H} and $^{31}$P{$^1$H} NMR spectra were recorded on a Bruker Avance III HD 500 MHz Smart Probe spectrometer using a BBO probe. $^1$H decoupling was achieved using the Waltz-16 decoupling sequence. $^1$H NMR spectra were internally referenced to DMSO-d$_6$ at 2.50 ppm and the $^{19}$F and $^{31}$P NMR spectra were internally reference to LiPF$_6$ at −74.5 ppm and −145 ppm, respectively.

## Results and Discussion

***NWO/LFP full cell at room temperature.***—To assess the stability of NWO anodes upon cycling, LFP cathodes, which are known to show stable cycling without significant degradation, were initially used in a full cell (1.54 mAh capacity). Figure 1a shows
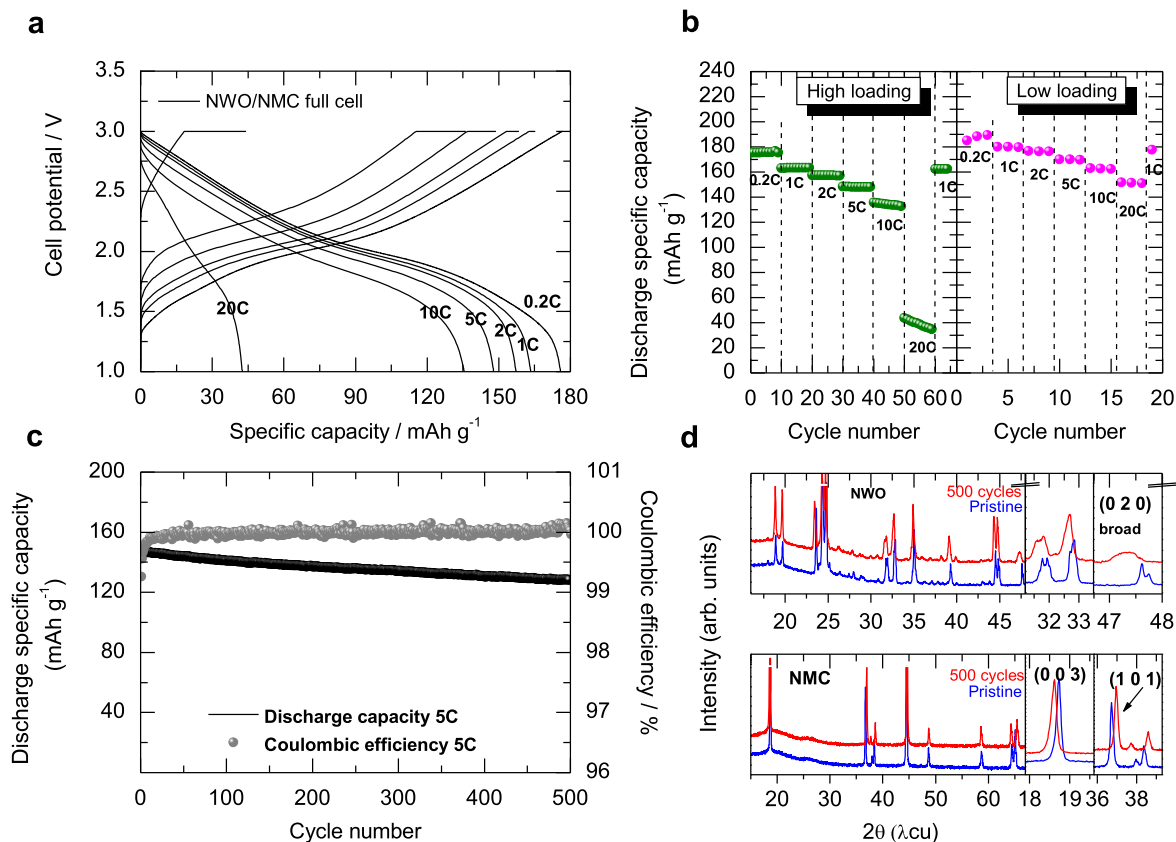
**Figure 2.** (a) Cell voltage profiles for the high loading NWO/NMC cell cycled at 0.2 C, 1 C, 2 C, 5 C and 10 C, (b) Rate performance of high loading and low loading NWO/NMC full cells. (c) Capacity retention and energy efficiency of the high loading NMC/NWO full cell cycled at 5 C. (d) XRD patterns of the pristine and ex situ NWO and NMC electrodes of a cell cycled at 5 C for 500 cycles and disassembled at the discharged state (i.e. lithiated NMC and delithiated NWO). Note that for the NWO, reflections along the (0k0) direction appear to be significantly broadened, which suggests an anisotropic microstructural change of particles.

the voltage profiles of the charge and discharge reaction, and the operating window was determined to be between 0.5 to 2.6 V, with >90.8% of the capacity being obtained between 1 and 2 V on discharge at C/5 (34.2 mA g$^{-1}$). Figure 1b shows the discharge capacity as a function of C-rate at 25 °C, the cells showing discharge capacities of 140 mAh g$^{-1}$ at 0.2 C and 130, 125, 112, 92 and 39 mAh g$^{-1}$ at 1 C, 2 C, 5 C, 10 C and 20 C, respectively. The cell recovers a capacity of 128 mAh/g when the C-rate is returned to 1 C. The discharge capacity of this NWO/LFP cell at 20 C is significantly reduced, but could be improved by optimizing the electrode structure as suggested by the C-rate performance of lower electrode loadings which delivers up to 89 mAh g$^{-1}$ at 20 C (Fig. 1b).

Based on this result, the long-term cycling performance of NWO/LFP cells was investigated for 1000 cycles at a rate of 5 C and 10 C over the full state-of-charge range. At 5 C, 92.1% of capacity retention is observed at 1000 cycles, 3.9% of the original capacity being lost after 100 cycles and 7.9% at 500 cycles (Fig. 1c). However, less than 0.01% capacity loss was observed during the final 500 cycles. In other words, after the initial 500 cycles, only 0.00002% of the capacity decays per cycle. The capacity retention was further checked by cycling the cell at 1 C after the initial 1000 cycles, the cell recovered 96.5% of the original capacity. Full cell operation at 10 C demonstrated capacity losses of 6.8%, 9.2% and 11.1% for 100, 500 and 1000 cycles, respectively; the corresponding coulombic efficiency remained constant at 99.99% up to 1000 cycles. Note that XRD patterns of the NWO electrode after 200 and 500 cycles at 5 C show that the crystal structure is retained with no peak broadening and signs of amorphization (Fig. 1d). These results clearly illustrate the excellent long-term cyclability of NWO/LFP full cells up to 1000 cycles, which directly demonstrates the applicability of NWO materials as anodes in Li-ion full cells.

At this stage we compare these cell performances with LTO/LFP full cells since LTO has a similar working voltage to NWO but is already commercialized in battery technology. Pohjalainen et al. have reported LTO/LFP full cells with a discharge capacity fade of 5% under 1 C for 300 cycles.[23] Wang et al. have reported that a carbon-modified LFP and unmodified LTO anode exhibited capacity loss of 11% at 0.5 C over more than 1200 cycles.[24] However, in another example, cells constructed with submicron spherical secondary LTO particles and commercial LFP achieved excellent performances (2% capacity loss for 8000 cycles at 30 C).[25] The present high loading NWO/LFP cells, without optimization of particle size, morphology, binder chemistry or electrolyte composition, shows comparable or better cycle life at higher C-rates than reported for many of these LTO/LFP cells. These results are extremely promising and call for further optimization to investigate the full potential of this chemistry.

***NWO/NMC full cell at room temperature.***—To further increase the energy density of the full cell, the NWO anode was tested against an NMC-622 cathode, which has emerged as a leading cathode for high energy density cells against a standard graphite anode.[26,27] The voltage windows of both electrodes were determined by using a three-electrode cell with a lithium metal reference electrode (Fig. S3a). Figure 2a shows the voltage profile of the NWO/NMC cell (1.78 mAh cell capacity). At a 0.2 C rate, it shows a discharge capacity of 175 mAh g$^{-1}$ in the working voltage range of 1–3 V, with > 91.6% of the capacity being accessed above 1.5 V and an initial coulombic efficiency of this NWO/NMC cell of 87.6% (Fig. S3b).

Figure 2b shows the discharge capacity as a function of C-rate obtained from the NWO/NMC cell. At 0.2 C, the cell showed
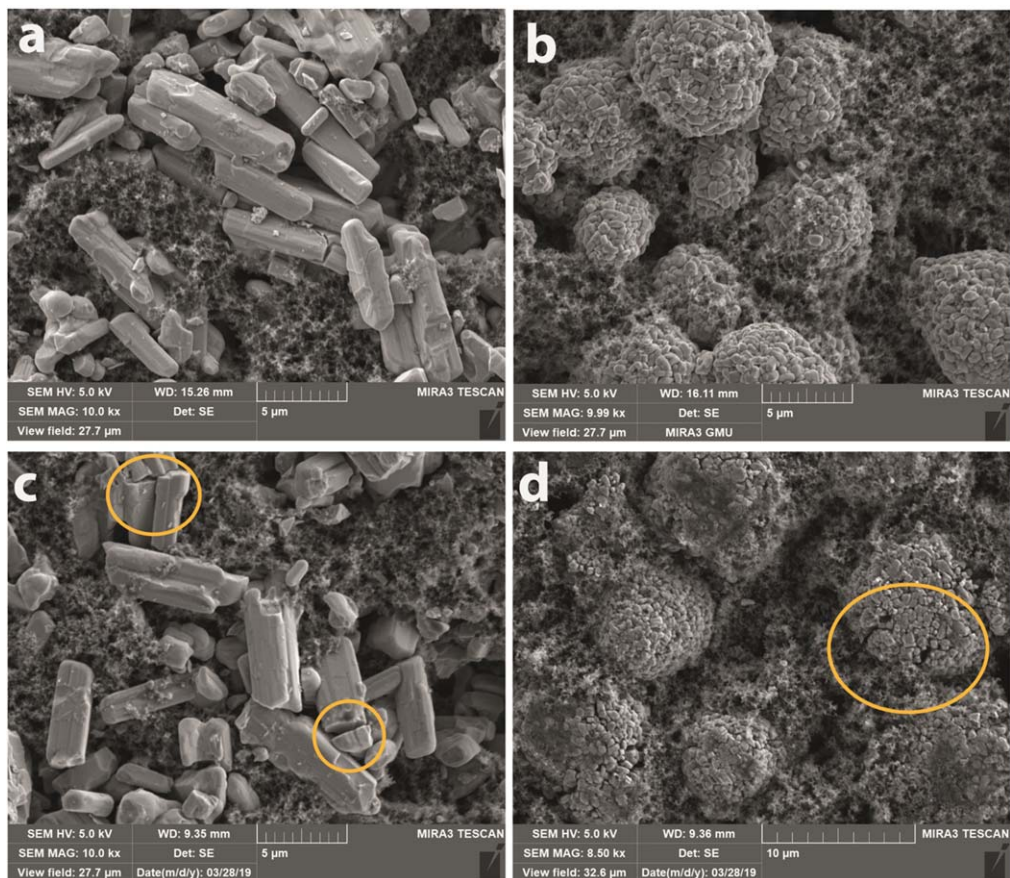
**Figure 3.** SEM images of the (a) pristine NWO, (b) pristine NMC, (c) 500 cycled NWO and d) 500 cycled NMC electrodes.
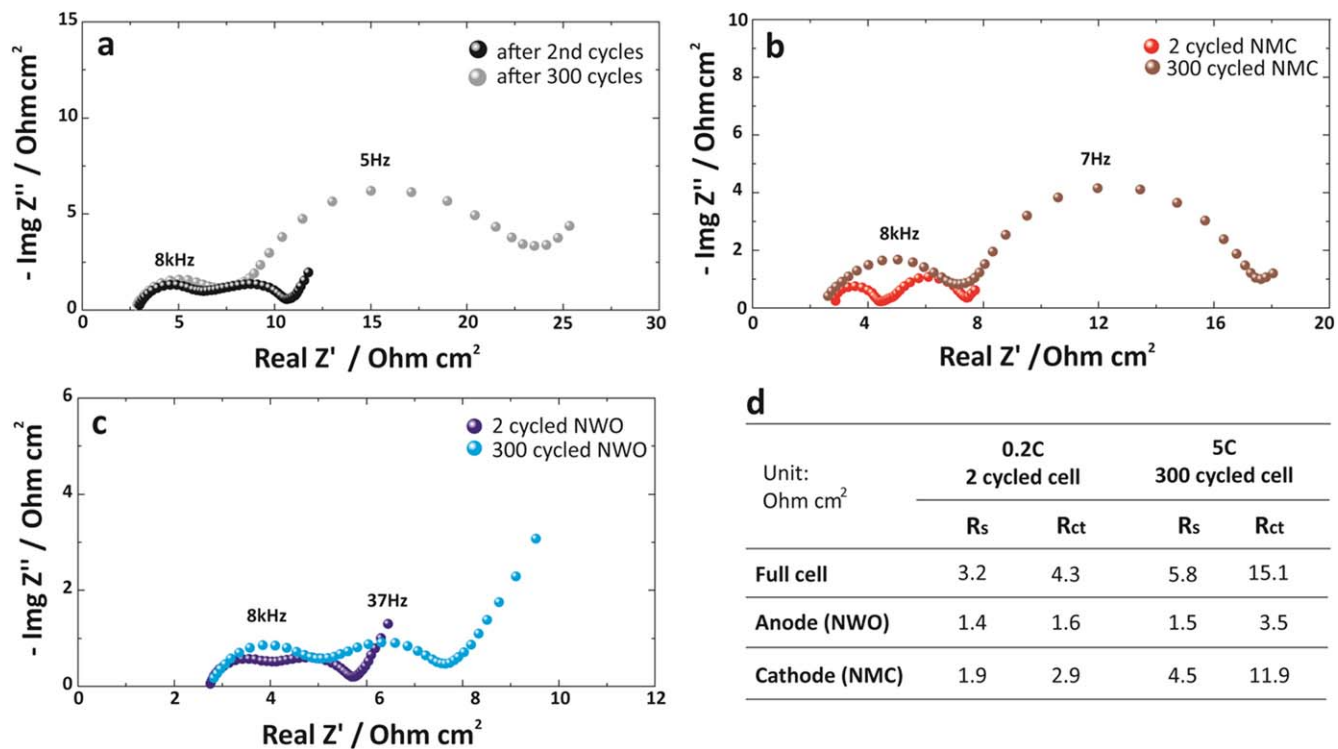


**Figure 4.** Nyquist plots of the (a) full cell after the 2nd and 300th cycles at 2 V during charging step, and Nyquist plots of the (b) symmetric NMC cell and (c) symmetric NWO cell from the full cell electrodes. (d) Fitting results from measured impedance by using the equivalent circuit shown in Fig. S6. In this study, bulk resistance which is affected by electrolyte solution resistance in the cell is manually shifted to the same number as different separators (polymer separator and glass fiber separator) were used for the full cells and half cells, respectively.
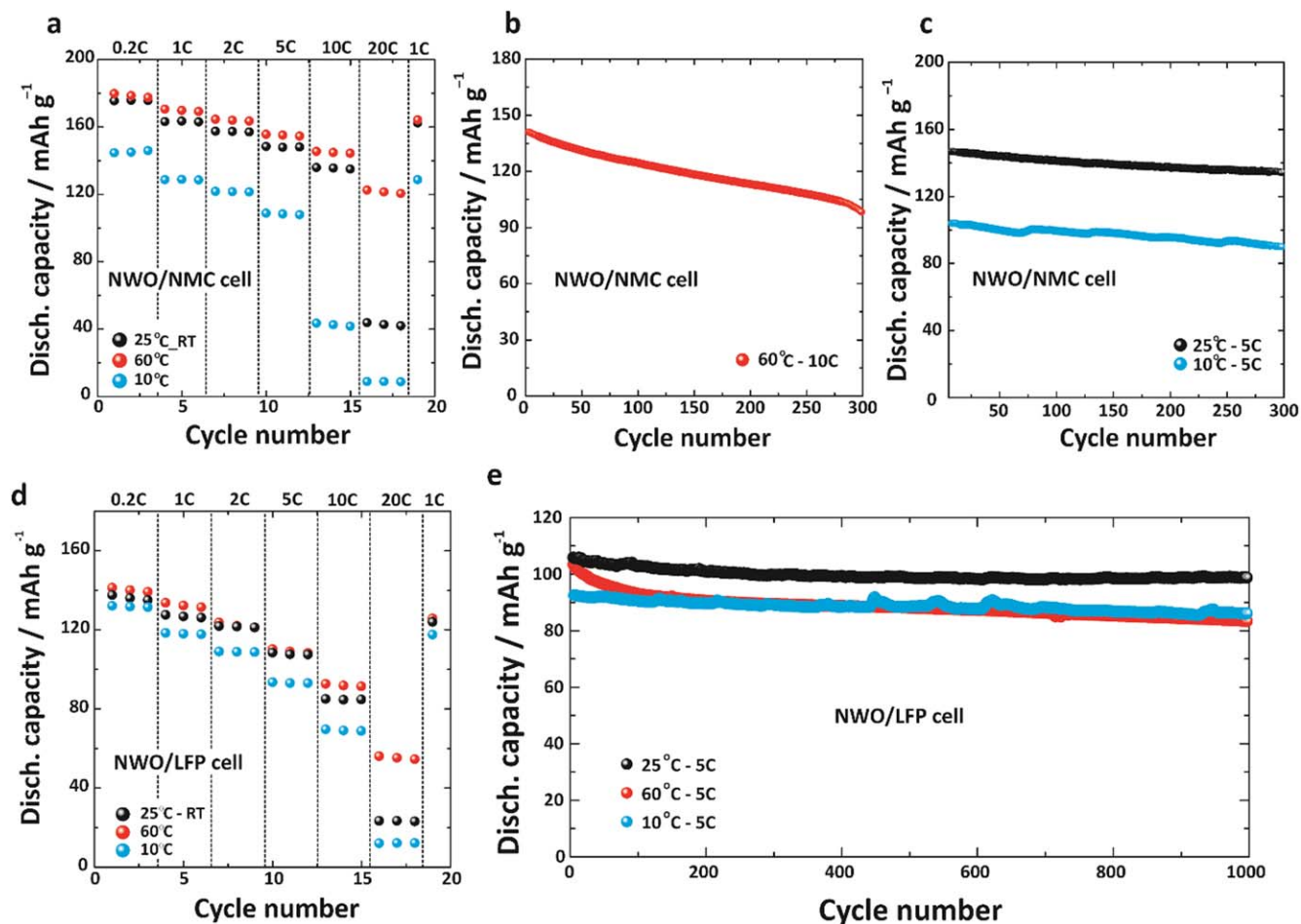
**Figure 5.** (a) Rate performance comparison as a function of the cell operation temperature (10, 25 °C and 60 °C). Long-term cycle performance of NWO/NMC cell (b) at 60 °C and 10 C rate and (c) at 10 °C and 25 °C at 5 C rate conditions. (d) Rate performance comparison of the NWO/LFP cells as a function of temperature and (e) long-term cycle performance at 10 °C, 25 °C, 60 °C at 5 C rate.

discharge capacity of 175 mAh g$^{-1}$, with the successively decreasing capacities of 163, 157, 148 and 136 mAh g$^{-1}$ at 1 C, 2 C, 5 C and 10 C, respectively. A noticeable drop in capacity to 43 mAh g$^{-1}$ was obtained upon 20 C cycling. Similarly, to the LFP/NWO full cell, we attribute this drop to kinetic limitation in the electrode since i) close to the initial capacity (162 mAh g$^{-1}$) could be recovered on returning to 1 C, and ii) 152 mAh g$^{-1}$ at 20 C is obtained for a full cell with a lower loading. Capacity retention and coulombic efficiency at 5 C for 500 cycles were 86.8% and 99.9%, respectively (Fig. 2c). This means a stable cycling performance with a 0.026% of capacity loss per cycle at a 5 C rate operation.

To gain further insights into the structural changes and the possible sources of the degradation of the NWO/NMC full cell, ex situ XRD and SEM analyses were conducted on the extracted electrodes from the cells that were cycled 500 times over the full state-of-charge range. The XRD pattern from the cycled NWO electrode (Fig. 2c) shows no indication of any new phases; however, the monoclinic lattice has expanded by 1.2% in comparison to that of the pristine material, according to Rietveld refinements (Fig. S4 and Table SI), most likely because of the presence of Li$^+$ in the structure.[17] On the NMC side (Fig. 2d), Rietveld refinement shows a shrinkage along the *a*- and *b*-direction and an elongation along the *c*-direction compared to the pristine material, which is consistent with Li deficiency.[28–31] Based on the volume changes, it can be proposed that, at the end of the 500th discharge, a quantity of lithium equivalent to 25 mAh g$^{-1}$ has not been removed from NWO while 42 mAh g$^{-1}$ is missing from the NMC (detailed in Table SI caption).

This suggests that the capacity loss is due to (i) active Li loss and (ii) accumulation of the Li in the NWO electrode.

To investigate the source of cell degradation further (NWO anode or NMC cathode), SEM images of the pristine and 500-cycled NWO anode are compared (Figs. 3a, 3c). The NWO particles having an elongated shape, due to a preferential growth of the crystal along the b direction, show several microcracks and a optically clean surface in both the pristine material and after cycling. On the other hand, SEM images (Figs. 3b, 3d) of the pristine and 500-cycled NMC cathodes demonstrate a clear partial destruction of the spherical particles. Particle cracking during cycling is a relatively well-known degradation phenomenon observed from NMC cathode materials; cracks on the particle surfaces can cause, or accelerate, the dissolution of transition metals such as Mn and Ni. Furthermore, the electrical contact between the active material and the conductive carbon can be lost resulting in degradation of the cell performance.[29,30,32]

Electrochemical impedance measurements were conducted in full cells and symmetric cells. Cell impedance was measured in symmetric cells which were assembled with electrodes taken from two full cells operated under the same conditions. Two sets of cells were prepared: one was tested after 2 cycles at 0.2 C and the other was tested after 300 cycles at 5 C. Figure 4a indicates the full cell impedance obtained after the 2nd and 300th cycles; Figs. 4b and 4c represent the cell impedance from cathode and anode symmetric cells, respectively. The data were fitted assuming an equivalent circuit[33] composed of the bulk resistance (R$_b$), electrode surface
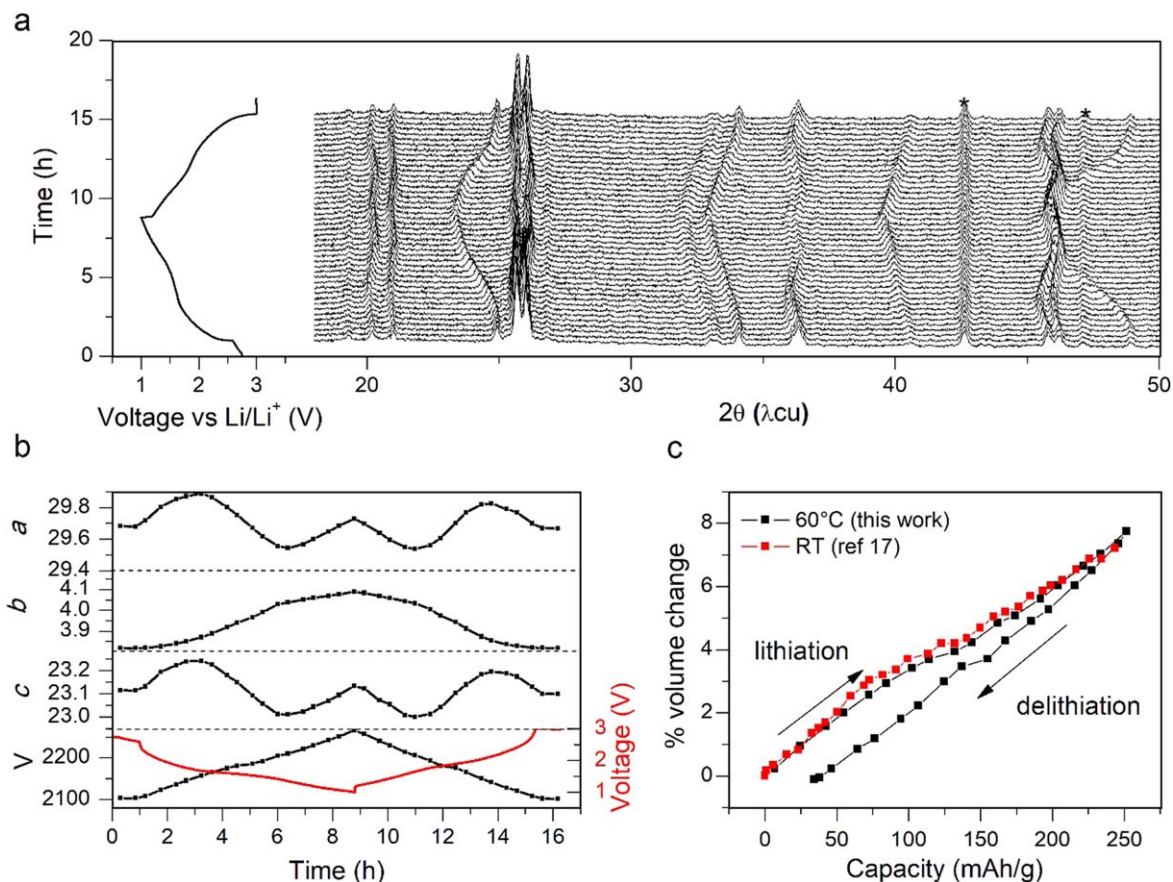
**Figure 6.** (a) XRD patterns obtained *operando* during the 1st cycle of a NWO half-cell at 60 °C and C/5 rate together with the galvanostatic profile on the left side. *beryllium window (b) Cell parameters in Å and unit cell volume in Å$^3$ together with the galvanostatic cycling data obtained from Lebail fit of the *operando* data. (c) Variation of the unit cell volume at room temperature and 60 °C in red and black, respectively.
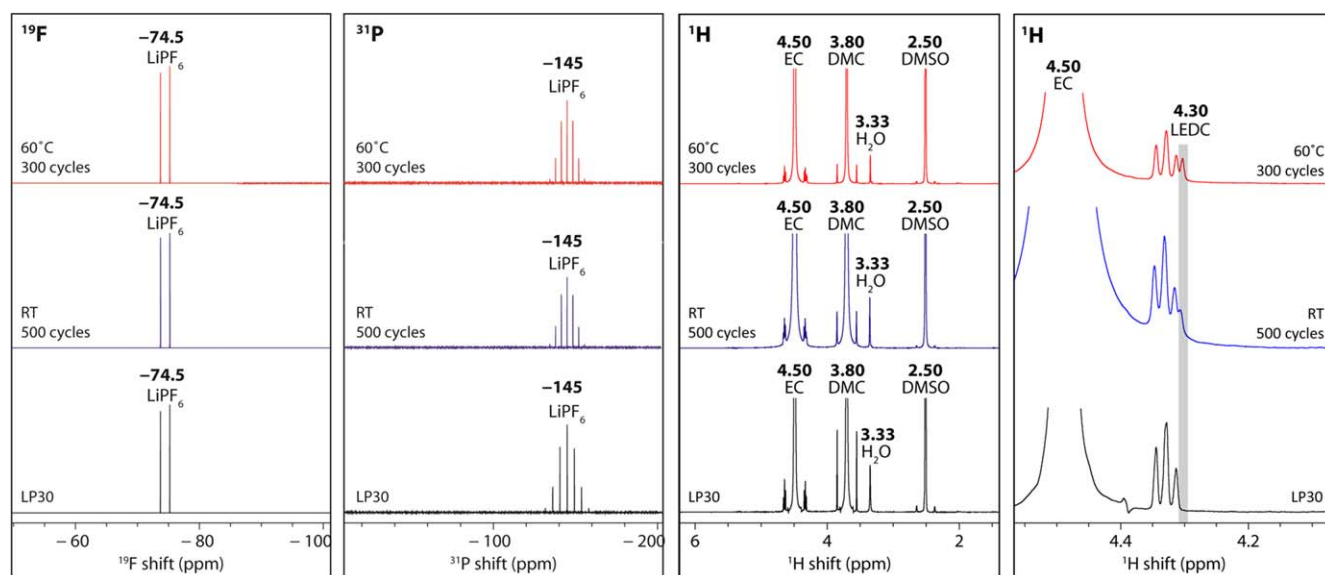


**Figure 7.** $^1$H, $^{19}$F, $^{31}$P solution NMR spectra of the electrolytes extracted from the cells (DMSO-$d_6$ solvent) cycled at a rate corresponding to 5 C for 300 cycles at 60 °C and for 500 cycles at 25 °C, and LP30 electrolyte as baseline. Note that the water peak likely originates from the DMSO solvent.

resistance ($R_s$) and charge transfer resistance ($R_{ct}$) as shown in Fig. S5; the fitted parameters are summarized in Fig. 4d. In a full cell, the increase in $R_{ct}$ upon cycling is the dominant source of the increase in overall cell impedance. By cycling the same electrode films in symmetric cells, the $R_{ct}$ in the NWO symmetric cell only increases from 1.6 to 3.5 $\Omega$ cm$^2$ while $R_{ct}$ in the NMC symmetric cell increases from 2.9 to 11.9 $\Omega$ cm$^2$. This indicates that the increase of the full cell resistance is mainly due to the increase in charge transfer resistance at the NMC cathode rather than at the NWO anode. Note that the increase of the charge transfer resistance at the
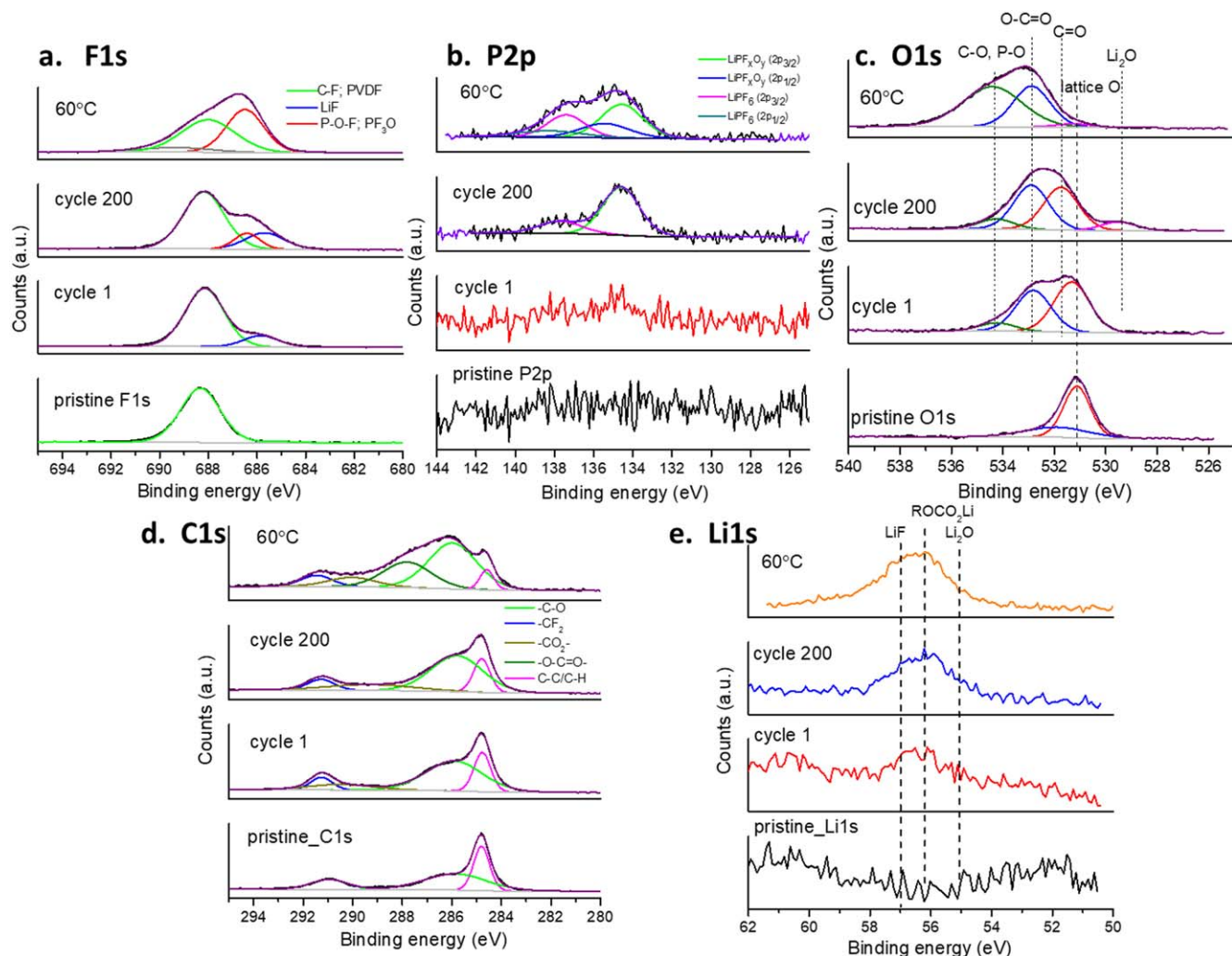
**Figure 8.** C 1*s*, F 1*s*, O 1*s*, P 2*p* and Li 1*s* X-ray photoelectron spectra NWO anode of NWO/NMC cells before and after cycling at 25 °C (200 cycles) and 60 °C (300 cycles). The fitted and measured spectra are marked with purple and black, respectively.

NMC cathode is consistent with previous literature and explanations for this include a loss of electrical contact by particle fracture and/or the formation of a resistive surface layer.[21,26,27]

*Temperature dependence of the NWO properties.*—Next, in order to evaluate the performance of the cell at different temperatures, NWO/NMC and NWO/LFP cells were tested at 10 °C, 25 °C and 60 °C (Fig. 5). The discharge capacities of the two cells tested at different C-rates at 60 °C and 10 °C show higher and lower relative values, respectively, as compared to the 25 °C cell, as expected from the thermal activation of the kinetics of charge transfer and diffusion. Long-term cycling performance of NWO/NMC was evaluated for 300 cycles under three different conditions: 10 C rate at 60 °C (Figs. 5b) and 5C rate at 10°C and 25 °C (Fig. 5c). Cell cycling at 60 °C (10 C rate) resulted in a loss of 30.8% of discharge capacity after 300 cycles while the cells at 25 °C (5 C rate) and 10 ° C (5 C rate) showed 9.2% and 15.5% capacity loss in the same cycling window. Variable-temperature cycling of NWO/LFP was conducted for 1000 cycles at 5 C rate. At temperatures of 10 °C, 25 °C and 60 °C (Figs. 5e), 6.9%, 7.9% and 18.1% capacity losses were observed over 1000 cycles, respectively. This indicates NWO is suitable at different temperatures and that the NWO/LFP combination has better cycling stability and operational temperature range than NWO/NMC with the electrolyte used here.

Owing to the excellent cycling stability of the LFP/NWO full cell at 60 °C, we conducted an *operando* XRD experiment at this temperature during the 1st cycle of a NWO half-cell at C/5 (Fig. 6a), and plotted the results of the Lebail refinements (Figs. 6b, 6c). A solid solution mechanism is observed across the full cycle, with an increase of the *b* parameter and a more complex variation of the *a* and *c* parameters. Such evolution is very similar to the room temperature behaviour from Ref. 17, as shown in Fig. 6c in which the trace of the unit cell volume variation during Li insertion/extraction at 60 °C is nearly superimposed with the one recorded at 25 °C. The similar structural evolution is consistent with the good cycling behaviour at 60 °C and also calls for the investigation of the temperature limit at which this material can cycle without structural decomposition.

*Electrolyte degradation in NWO full cells.*—To understand the degradation of the electrolyte during full cell cycling, NMR and XPS analyses were carried out to track the presence of dissolved and surface species, respectively.

^{1}H, ^{19}F and ^{31}P NMR spectra of the electrolyte extracted from NWO/NMC cells cycled at 5 C for 300 cycles at 60 °C and 500 cycles at 25 °C are compared to the spectra of a pristine electrolyte (Fig. 7). On the ^{19}F and ^{31}P spectra no extra peaks are observed after cycling. The ^{1}H spectra of the cycled samples present a small peak at 4.3 ppm originating from trace quantities of lithium ethylene dicarbonate (LEDC) likely due to hydrolysis of EC with trace moisture. Integration of the ^{1}H peak area gives an estimated content of LEDC:EC as 0.1 mol.% (300 cycles, 60 °C) and 0.05 mol.% (500 cycles, 25 °C).

F 1*s*, C 1*s*, O 1*s*, Li 1*s* and P 2*p* photoelectron spectra of NWO anode from cycled NWO/NMC cells (Fig. 8) show the presence of surface species after cycling at room temperature (200 cycles) as well as 60 °C (300 cycles). The F 1*s* spectra show that LiF forms after the 1st cycle but does not change significantly after 200 cycles (Fig. 8a). However, a new peak appears around 686.4 eV due to $PO_xF_y$ species after 200 cycles, presumably arising from the degradation of $LiPF_6$ via reaction with moisture or oxygen.[34,35] Formation of $PO_xF_y$ species is also confirmed by P 2*p* spectra[36] after cycling at room temperature (Fig. 8b). On cycling at 60 °C, the extent of $LiPF_6$ degradation has increased, as seen by a significant rise in both the F 1*s* and the P 2*p* XPS intensity due to $PO_xF_y$ components. In addition, the O 1*s* spectra for the 60 °C cycled sample shows a large increase in peak intensity at 534.4 eV arising from singly-bonded oxygen moieties, including P–O species[37] (Fig. 8c). The C 1*s* and O 1*s* spectra show that the increase in intensity of C–O and C=O species at the end of cycling could be due to the accumulation of alkyl carbonate and lithium carbonate species (Figs. 6c and 6d). C 1*s* XPS of the 60 °C cycled sample shows an intense peak around 288.9 eV assigned to O–C=O bonds,[36] likely to be originating from lithium ethylene dicarbonate (LEDC) as also observed in the NMR studies. Li 1*s* shows a broad band from 54–58 eV that includes contributions from LiF and $ROCO_2Li$ surface species (Fig. 8e).[36] A trace amount of $Li_2O$ is detected by O 1*s* and Li 1*s* spectra after long-term cycling at room temperature.

Overall, it can be concluded that i) a very small amount of EC is being reduced at the NWO surface leading to a trace amount of LEDC in the electrolyte and the accumulation of lithium alkyl carbonate at the surface of electrode, ii) residual water leads to the formation of $LiPF_6$ decomposition products such as deposited $PO_xF_y$ species and soluble $[PO_2F_2]^-$.[38,39] This suggests only minor electrolyte decomposition even in the absence of additives.

## Conclusions

This work demonstrates the feasibility of utilizing NWO anodes with two commercial cathodes (LFP, NMC-622) for Li-ion batteries; it also represents a step forward in terms of finding the optimum cell components (cathode, electrolyte) to fully realize the high-rate electrochemical capabilities of NWO. NWO/LFP cells show an 88.9% capacity retention at 10 C rate for 1000 cycles and NWO/NMC cells show 86.8% capacity retention at 5 C rate for 500 cycles. Even at 10 °C and 60 °C, NWO/NMC cells operate well up to 5 C rate and 20 C rate, respectively. The slight degradation of the cell performance that does occur mainly comes from the degradation of NMC cathodes, as shown from the cell impedance measurements. The stable and fast electrochemical performance shown here by anodes with bulk NWO particles, shows that these cells represent feasible and promising candidates for high rate lithium ion batteries.

## Acknowledgments

## ORCID

Yumi Kim https://orcid.org/0000-0001-6675-7522
Quentin Jacquet https://orcid.org/0000-0002-3684-9423
Kent J. Griffith https://orcid.org/0000-0002-8096-906X

## References

1. M. Li, J. Lu, Z. Chen, and K. Amine, *Adv. Mater.*, **30**, 1800561 (2018).
2. N. Nitta, F. Wu, J. T. Lee, and G. Yushin, *Mater. Today*, **18**, 252 (2015).
3. S. Goriparti, E. Miele, F. De Angelis, E. Di Fabrizio, R. Proietti Zaccaria, and C. Capiglia, *J. Power Sources*, **257**, 421 (2014).
4. K. Kang, Y. S. Meng, J. Bréger, C. P. Grey, and G. Ceder, *Science*, **311**, 977 (2006).
5. S. W. Lee, N. Yabuuchi, B. M. Gallant, S. Chen, B.-S. Kim, P. T. Hammond, and Y. Shao-Horn, *Nat. Nanotechnol.*, **5**, 531 (2010).
6. A. Kraytsberg and Y. Ein-Eli, *Adv. Energy Mater.*, **2**, 922 (2012).
7. B. Scrosati and J. Garche, *J. Power Sources*, **195**, 2419 (2010).
8. B. Wang, W. A. Abdulla, D. Wang, and X. S. Zhao, *Energy Environ. Sci.*, **8**, 869 (2015).
9. F. Lin, I. M. Markus, D. Nordlund, T.-C. Weng, M. D. Asta, H. L. Xin, and M. M. Doeff, *Nat. Commun.*, **5**, 3529 (2014).
10. P. Rozier and J. M. Tarascon, *J. Electrochem. Soc.*, **162**, A2490 (2015).
11. V. A. Agubra and J. W. Fergus, *J. Power Sources,*, **268**, 153 (2014).
12. S. An, J. Li, C. Daniel, D. Mohanty, S. Nagpure, and D. L. Wood III, *Carbon*, **105**, 52 (2016).
13. G.-N. Zhu, H.-J. Liu, J.-H. Zhuang, C.-X. Wang, C.-G. Wang, and Y.-Y. Xia, *Energy Environ. Sci.*, **4**, 4016 (2011).
14. I. Belharouak, G. M. Koenig, and K. Amine, *J. Power Sources*, **196**, 10344 (2011).
15. Y.-B. He et al., *Sci. Rep.*, **2**, 913 (2012).
16. I. Belharouak, G. M. Koenig, T. Tan, H. Yumoto, N. Ota, and K. Amine, *J. Electrochem. Soc.*, **159**, A1165 (2012).
17. K. J. Griffith, K. M. Wiaderek, G. Cibin, L. E. Marbella, and C. P. Grey, *Nature*, **559**, 556 (2018).
18. C. Yang et al., *J. Power Sources*, **360**, 470 (2017).
19. L. Yan, H. Lan, H. Yu, S. Qian, X. Cheng, N. Long, R. Zhang, M. Shui, and J. Shu, *J. Mater. Chem. A*, **5**, 8972 (2017).
20. Q. Cheng, J. Liang, N. Lin, C. Guo, Y. Zhu, and Y. Qian, *Electrochim. Acta*, **176**, 456 (2015).
21. B. Guo, X. Yu, X.-G. Sun, M. Chi, Z.-A. Qiao, J. Liu, Y.-S. Hu, X.-Q. Yang, J. B. Goodenough, and S. Dai, *Energy Environ. Sci.*, **7**, 2220 (2014).
22. J. Rodríguez-Carvajal, *Physica B*, **192**, 55 (1993).
23. E. Pohjalainen, T. Rauhala, M. Valkeapää, J. Kallioinen, and T. Kallio, *J. Phys. Chem.*, **119**, 2277 (2015).
24. W. Wang, D. Choi, and Z. Yang, *Metall. Mater. Trans. A*, **44A**, S21 (2013).
25. C. Wang et al., *Chem. Mater.*, **27**, 5647 (2015).
26. G. E. Blomgren, *J. Electrochem. Soc.*, **164**, A5019 (2017).
27. G. Zubi, R. Dufo-López, M. Carvalho, and G. Pasaoglu, *Renew. Sust. Energ. Rev.*, **89**, 292 (2018).
28. J. Li, L. E. Downie, L. Ma, W. Qiu, and J. R. Dahn, *J. Electrochem. Soc.*, **162**, A1401 (2015).
29. P.-C. Tsai, B. Wen, M. Wolfman, M.-J. Choe, M. S. Pan, L. Su, K. Thornton, J. Cabana, and Y.-M. Chiang, *Energy Environ. Sci.*, **11**, 860 (2018).
30. M. Ebner, F. Geldmacher, F. Marone, M. Stampanoni, and V. Wood, *Adv. Energy Mater.*, **3**, 845 (2013).
31. I. Buchberger, S. Seidlmayer, A. Pokharel, M. Piana, J. Hattendorff, P. Kudejova, R. Gilles, and H. A. Gasteiger, *J. Electrochem. Soc.*, **162**, A2737 (2015).
32. P. Yan, J. Zheng, M. Gu, J. Xiao, J.-G. Zhang, and C.-M. Wang, *Nat. Commun.*, **8**, 14101 (2017).
33. S. S. Zhang, K. Xu, and T. R. Jow, *Electrochim. Acta*, **49**, 1057 (2004).
34. G. M. Veith and N. J. Dudney, *J. Electrochem. Soc.*, **158**, A658 (2011).
35. H. Ota, X. Wang, and E. Yasukawa, *J. Electrochem. Soc.*, **151**, A437 (2004).
36. D. Aurbach, B. Markovsky, A. Shechter, Y. E. Eli, and H. Cohen, *J. Electrochem. Soc.*, **143**, 3809 (1996).
37. N. Schulz, R. Hausbrand, C. Wittich, L. Dimesso, and W. Jaegermann, *J. Electrochem. Soc.*, **165**, A833 (2018).
38. B. S. Parimalam, A. D. MacIntosh, R. Kadam, and B. L. Lucht, *J. Phys. Chem.*, **121**, 22733 (2017).
39. M. Stich, M. Göttlinger, M. Kurniawan, U. Schmidt, and A. Bund, *J. Phys. Chem.*, **122**, 16 (2018).